ADVANCED OPTICAL MATERIALS
www.advopticalmat.de

Ultrastrong Coupling of Electrically Pumped Near-Infrared Exciton-Polaritons in High Mobility Polymers

Martin Held, Arko Graf, Yuriy Zakharko, Pengning Chao, Laura Tropf, Malte C. Gather, and Jana Zaumseil**

Exciton-polaritons are quasiparticles with hybrid light–matter properties that may be used in new optoelectronic devices. Here, electrically pumped ultrastrongly coupled exciton-polaritons in a high-mobility donor–acceptor copolymer are demonstrated by integrating a light-emitting field-effect transistor into a metal-clad microcavity. Near-infrared electroluminescence is emitted exclusively from the lower polariton branch, which indicates efficient relaxation. A coupling strength of 24% of the exciton transition energy implies the system is in the ultrastrong coupling regime with a narrow and almost angle-independent emission. The lower polariton energy, which can be adjusted by the cavity detuning, strongly influences the external quantum efficiency of the device. Driving the transistors at ambipolar current densities of up to 4000 A cm^{-2} does not decrease the coupling strength or polariton emission efficiency. Cavity-integrated light-emitting field-effect transistors thus represent a versatile platform for polariton emission and polaritonic devices.

1. Introduction

Exciton-polaritons are hybrid light–matter particles that are formed when the coupling rate between the excited state of an emitter (exciton) and the surrounding cavity mode (photon) exceeds their rate of dissipation. In this strong coupling regime, two new hybridized modes appear—the upper (UP) and lower polariton (LP). These manifest in a characteristic anticrossing of the almost dispersionless exciton and the parabolic photon dispersion. From the dispersion of the polariton modes, the coupling potential (V_A), which is proportional to the observed minimal splitting between UP and LP, can be deduced. Organic materials favor particularly high coupling potentials ($V_A > 100$ meV) due to their large oscillator strength and are ideal to create exciton-polaritons at room-temperature due to their large exciton binding energies.[1–4] The unique combination of both light and matter character in exciton-polaritons results in fascinating properties, for example, polaritons can reach a macroscopic occupation of the ground state (condensation) at room-temperature with coherent light emission, so-called polariton lasing, at lower thresholds than conventional photon lasing.[5–9] They may also affect chemical reactions and there have been suggestions that they can even influence charge transport.[10,11]

Polariton emission typically occurs from the LP branch due to relaxation enabled by the excitonic character of the polaritons. Owing to their hybrid excitonic–photonic character, the emission linewidth of the LP is typically narrowed for many organic systems and can be spectrally tuned by adjusting the cavity resonance.[4] Further, if the coupling potential of the hybrid system exceeds about 20% of the exciton energy, the regime of ultrastrong coupling is reached, for which new intriguing phenomena are predicted and have also been observed to some extent.[12–15] Emission from the lower polariton in the ultrastrong coupling regime shows very low dispersion and thus minimal angular color shift while maintaining the narrow linewidth of the mixed state.[13,16] This feature makes the ultrastrong coupling regime attractive for color-pure emission from electrically driven light-emitting devices. Semiconducting donor–acceptor polymers show unusually high oscillator strength at low photon energies[17] and are thus ideal materials to achieve ultrastrong coupling. At the same time these polymers exhibit large ambipolar charge carrier mobilities, which render them interesting for electrical generation of exciton-polaritons.[18,19]

In previous work light-emitting diode (LED) structures were used to achieve electrically driven exciton-polariton emission. In these structures, the cavity mirrors also acted as the injection electrodes.[15,20–24] In case of organic LEDs (OLEDs), metallic anodes and cathodes (e.g., silver or aluminum) were

M. Held, A. Graf, Dr. Y. Zakharko, Prof. J. Zaumseil
Institute for Physical Chemistry
Universität Heidelberg
D-69120 Heidelberg, Germany
E-mail: zaumseil@uni-heidelberg.de
P. Chao
Department of Electrical Engineering
Princeton University
Princeton, NJ 08544, USA
L. Tropf, Prof. M. C. Gather
Organic Semiconductor Centre
SUPA
School of Physics and Astronomy
University of St Andrews
St Andrews KY16 9SS, UK
E-mail: mcg6@st-andrews.ac.uk
The ORCID identification number(s) for the author(s) of this article can be found under https://doi.org/10.1002/adom.201700962.

DOI: 10.1002/adom.201700962

used and electroluminescence was observed in the strong and ultrastrong coupling regime.[15,20–25] It is desirable to drastically increase the polariton densities reached under electrical pumping, potentially to levels that may enable polariton lasing. For this, it would be ideal to separate charge injection/transport and optical feedback so that each can be optimized independently. We have recently shown that this is possible in an ambipolar cavity-integrated light-emitting field-effect geometry using dense networks of semiconducting single-walled carbon nanotubes as a proof-of-principle.[26] Here, we demonstrate exciton-polariton electroluminescence from such a cavity-integrated light-emitting field-effect transistor (c-LEFET) with a high-mobility, near-infrared emitting donor–acceptor polymer (DPPT-BT) and show ultrastrong coupling. The c-LEFET structure allows us to tune the optical microcavity while independently optimizing charge injection and transport to reach high current densities. We demonstrate ultrastrong coupling of 314 meV (24% of the exciton transition energy), narrow polariton emission (full width at half maximum, FWHM = 46 nm) and a minimal energy (color) shift for a wide range of angles. The c-LEFETs also enable us to directly examine the impact of the cavity on charge transport in these polymers.

2. Results and Discussion

We employed the low bandgap diketopyrrolopyrole copolymer DPPT-BT (see **Figure 1**a, inset) as the semiconductor for charge transport and emission. DPPT-BT is a well-known donor–acceptor polymer[19,27,28] that exhibits an excitonic absorption maximum at 1.31 eV (945 nm) and an emission maximum at 1.18 eV (1050 nm) (Figure 1a). The low photoluminescence quantum yield (0.05%[18]) is typical for organic near-infrared emitters. Similar to other low-bandgap, donor–acceptor polymers, DPPT-BT has a high oscillator strength. The underlying large persistence length and torsional stiffness of these conjugated polymer chains[17] also give rise to high charge carrier mobilities.[29] Hole and electron mobilities for DPPT-BT field-effect transistors reach up to 0.6 $cm^2\ V^{-1}\ s^{-1}$.[18,19] We previously showed that the electroluminescence properties of DPPT-BT can be tuned and enhanced by plasmonic nanostructures in LEFETs without affecting their charge transport properties.[30,31] Further, in a spin-coated thin film of DPPT-BT the polymer chains and thus the transition dipoles are mainly oriented in-plane, resulting in a strongly anisotropic refractive index (Figure S1, Supporting Information) and thus increased outcoupling efficiency. These properties make DPPT-BT a good model system to study electrically pumped polariton emission in the strong and even ultrastrong coupling regime.

Here we used an ambipolar LEFET structure[32] and integrated it in a planar Fabry–Pérot microcavity as schematically shown in Figure 1b. After evaporation of the gold bottom mirror on a glass substrate, an insulating AlO_x spacer layer was deposited, gold source and drain electrode were patterned, followed by spin-coating of the DPPT-BT, deposition of the hybrid poly[methyl methacrylate](PMMA)/hafnium oxide (HfO_x) dielectric and a silver top gate that also acted as the top mirror. The cavity resonance was tuned by adjusting the thickness of the AlO_x spacer layer. In an LEFET with an ambipolar semiconductor such as DPPT-BT, both holes and electrons are injected and accumulated under appropriate biasing conditions,[33,34] which leads to the characteristic V-shaped transfer curves (Figure 1c). No additional charge injection or blocking layers are necessary. The hole and electron accumulation layers meet within the channel, excitons are generated and a narrow emission zone forms parallel to the source and drain electrodes (Figure 1b, bottom). By changing the applied voltages, the emission zone can be positioned throughout the entire channel (Movie S1, Supporting Information). All injected charges recombine and create excitons and thus we can directly determine the exciton density from the source–drain current and the emission zone width and depth.[31] Due to the high charge carrier mobilities in DPPT-BT (≈0.5 $cm^2\ V^{-1}\ s^{-1}$) ambipolar currents corresponding to current densities of up to 4000 A cm^{-2} were reached (see Experimental Section).

The DPPT-BT layer position and thickness in the c-LEFETs were optimized for electrical and optical performance. The latter is maximized by placing the emitter in the center of the cavity for highest electric field overlap while a thin dielectric layer is essential for driving the transistor at low gate voltages. The emission layer should be as thick as possible for maximum exciton-cavity coupling strength. However, thinner semiconducting layers reduce the vertical bulk resistance for charge injection,

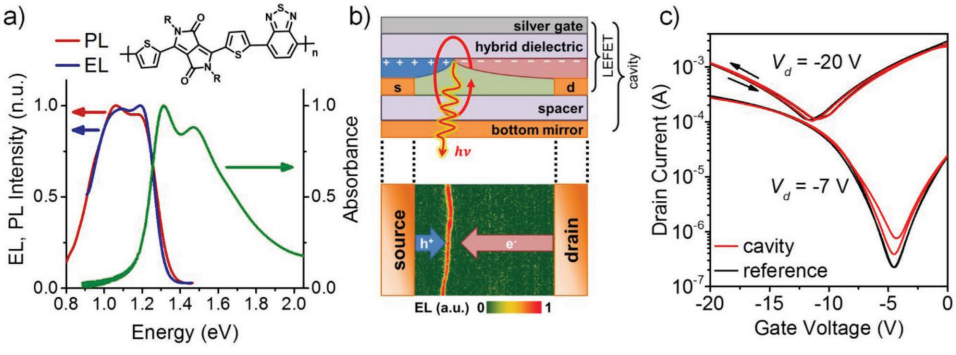

Figure 1. a) Absorption, photoluminescence (PL) and electroluminescence (EL) spectrum of the DPPT-BT polymer (inset: molecular structure). b, top) Schematic side-view and operation principle of a cavity-integrated ambipolar light-emitting field-effect transistor (c-LEFET). Holes (+) and electrons (–) are injected from the source (s) and drain (d) electrode, respectively. Excitons are formed and light is emitted ($h\nu$) from the c-LEFET. b, bottom) Real space image of the emission zone. c) Transfer curves of a c-LEFET (red) and a reference transistor (black, without bottom mirror/cavity) with L = 20 µm, W = 10 mm.

i.e., decrease contact resistance, in a top-gate geometry. A DPPT-BT film thickness of 60 or 39 nm and a hybrid dielectric layer of 11 nm PMMA and 51 nm HfO_x were found to fulfill these requirements. A direct comparison of a cavity-integrated LEFET to an LEFET without a bottom mirror and thus without a microcavity is shown in Figure 1c. In both cases ambipolar transport was observed. Neither the spacer layer nor the integration of the bottom mirror (not contacted, i.e., floating) significantly changed charge injection or ambipolar charge transport.

We investigated light–matter coupling in our c-LEFET structure by measuring the angle- and spectrally resolved reflectivity and emission. **Figure 2**a shows the reflectivity of the cavity from 1.0 to 1.8 eV, thus spanning the red to near-infrared wavelength range (for cross-sections at different angles and TM-mode see Figure S2a,b, Supporting Information). These images were acquired by combining data obtained with a back-illuminated CCD camera (>1.35 eV) and an InGaAs camera (<1.35 eV) from the exact same sample spot (see Experimental Section). Two new modes—above and below the exciton energy (X)—are clearly visible, indicating the UP and LP. In order to determine the coupling strength, both branches were fitted with the coupled oscillator model (see Experimental Section). The fit gave a coupling potential V_A of 314 meV, a cavity detuning of +80 meV, and an effective refractive index of 1.55. The coupling potential reached 24% of the exciton energy, thus placing the system in the ultrastrong coupling regime. A cavity quality factor of 40 was measured for an equivalent cavity, where the DPPT-BT was replaced with PMMA. While the LP branch is very narrow with only minimal dispersion, the UP branch is broadened due to the decreasing reflectivity of gold at wavelengths below 800 nm. The angle-dependent photoluminescence (PL) spectrum from the channel region of the c-LEFET (Figure 2b) shows polariton emission exclusively from the LP branch. The emission also perfectly matches the reflectivity minimum in forward direction (see Figure 2a). No purely excitonic emission was observed indicating that the emitting layer was coupled to the cavity. The same device exhibited electroluminescence (EL) from within the channel region that also closely followed the reflectivity minimum and thus the LP branch (Figure 2c). For this measurement a drain and gate bias of –20 V and –8 V, respectively, were applied (drain current I_d = 10 mA), resulting in an ambipolar current density of ≈500 A cm^{-2} (see Experimental Section). The narrow observable width of the emission zone (<1.1 µm) gives a high polariton pumping density; a pump rate of 3×10^{25} s^{-1} cm^{-3} was estimated (see Experimental Section) from this value, exceeding the pumping rates in previous cavity OLEDs.[20,21,23] The EL spectrum showed a slight broadening compared to the PL ($FWHM_{EL}$ = 55 meV vs. $FWHM_{PL}$ = 49 meV in forward direction). This deviation probably results from the fact that the EL was acquired from the whole field of view (400×400 µm^2) and thus from multiple channels (interdigitated electrodes) with slightly different cavity thicknesses simultaneously. We estimate the homogeneity of our multilayer stack and thus cavity thickness to be within ± 6.4 nm (i.e., ± 3% of a 218 nm stack) across the field of view. Emission with transverse magnetic polarization (TM, Figure S2c,d, Supporting Information) showed similar behavior.

From the coupled oscillator model fit, the excitonic and photonic fractions of the upper polariton and lower polariton branches were obtained (Figure 2d). A significant light–matter hybridization can be observed for all angles (±50°). Characteristically for the ultrastrong coupling regime, the excitonic fraction of the LP does not change strongly between large and small angles (86% at 50° compared to 61% at 0°). The EL emission intensity at a given energy, divided by the photon fraction, is also a direct probe of the occupancy along the LP branch and thus provides insight into polariton relaxation.[35] Under electrical pumping we observe a Boltzmann-like distribution of the LP around $k = 0$, which indicates thermalization of the polaritons in the LP branch and corroborates the absence of a relaxation bottleneck (Figure S3, Supporting Information). Thus, we achieved efficient relaxation from the exciton reservoir into the LP branch and toward $k = 0$ under electrical pumping in c-LEFETs.

Polaritonic emission in the ultrastrong coupling regime combines several desirable light emission features.[16] First, the cavity resonance is spectrally narrower than the excitonic emission of organic materials, hence the resulting polariton emission also becomes very narrow, as shown in **Figure 3**a. The electroluminescence spectrum of the lower polariton exhibits a 6.5 times narrower FWHM than the uncoupled excitonic emission (see also **Table 1**). Second, ultrastrong coupling results in a very flat dispersion of the lower polariton branch and thus PL and EL with a small energy shift of only 10 meV for emission angles from 0° to 40° (Figure 3b and Table 1). Compared to the

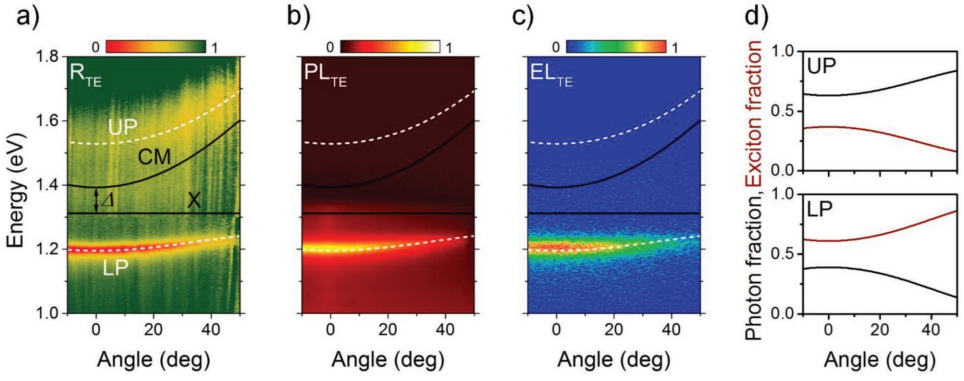

Figure 2. Angle- and spectrally resolved a) reflectivity (R), b) photoluminescence (PL), and c) electroluminescence (EL) for TE polarization of a c-LEFET with $E_{LP} - E_X = -116$ meV ($\Delta = 80$ meV detuning). The upper (UP) and lower (LP) polariton (white dashed lines), exciton (X) and cavity mode (CM) (black solid lines) branches were determined by the coupled oscillator model. d) Calculated photonic (black) and excitonic (red) fractions for the upper and lower polariton.

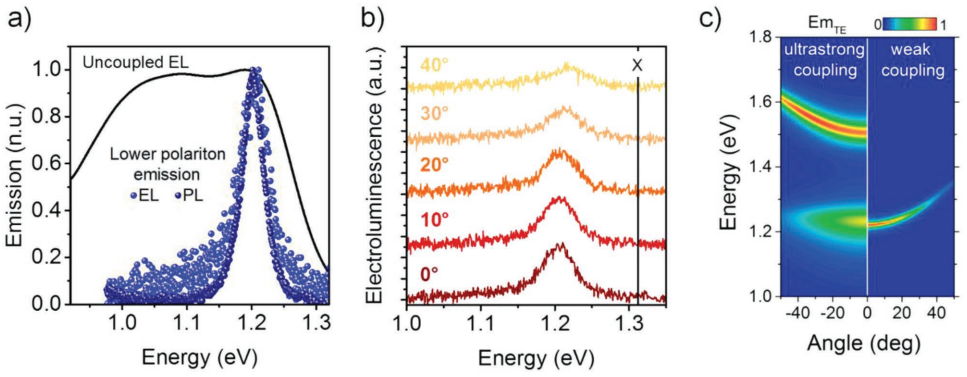

Figure 3. a) Comparison of the exciton-polariton PL and EL of a c-LEFET with $E_{LP} - E_X = -116$ meV ($\Delta = 80$ meV detuning) in forward direction with the uncoupled excitonic EL spectrum. b) Energy shift of the polariton EL for increasing detection angles. The X indicates the excitonic absorption maximum of the uncoupled emitter. c) Simulated emission from a c-LEFET under ultrastrong and weak coupling conditions for the same emission energy in forward direction (TE polarized spectral radiant intensity), indicating a much larger energy (color) shift for weak coupling.

corresponding cavity mode (Figure 2) with an energy shift of 140 meV, this is a reduction by a factor of 14.

In order to verify that this reduction originates from ultrastrong coupling, we simulated the angle-dependent reflectivity of a cavity in the weak coupling regime with the same emission energy (1.2 eV at $k = 0$) using the transfer matrix method. To ensure weak coupling, a stack with a 175 nm AlO_x spacer and 1 nm DPPT-BT emitter layer (same dielectric layer and mirrors as the c-LEFETs) was assumed (Figure S4a, Supporting Information). After increasing the thickness of the active polymer layer to 39 nm, ultrastrong light–matter hybridization—as observed in Figure 2a—was obtained for a 78 nm thick AlO_x layer. The strong coupling case closely reproduces our experimental dispersion data (Table S1, Supporting Information). The energy shift in the ultrastrong coupling regime is more than 20 times lower at an emission angle of 50° than under weak coupling conditions (Figure S4b,c and Table S1, Supporting Information).

Combining the transfer matrix method with an electromagnetic dipole model also allows us to simulate the outcoupled light of a dipole emitter from the cavity.[36] This is shown in Figure 3c, employing the same stacks as above and the experimental uncoupled EL spectrum of DPPT-BT (Figure 3c). In both cases, the emission follows the modes as seen in reflectivity. The discrepancy in intensity between the simulated emission and our experimental findings can be attributed to polariton relaxation mechanisms (scattering to the LP) that are not included in the purely optical simulation.

In order to investigate the influence of the energetic position E_{LP} of the lower polariton on the resulting emission (**Figure 4**a), with respect to the exciton E_X in forward direction as $E_{LP} - E_X$, we varied the AlO_x spacer thickness of the c-LEFET and thus the cavity detuning (Table S2, Supporting Information). We fabricated several c-LEFETs with $E_{LP} - E_X$ values ranging from −163 to −91 meV. For all of the devices the angular reflectivity and emission spectra showed ultrastrong coupling and emission exclusively from the LP branch (Figure S5, Supporting Information). A red-shift of the LP (increasing $E_{LP} - E_X$) increased the photonic character (Figure S5g–k, Supporting Information) and reduced the FWHM of the emission in forward direction from ≈50 to ≈30 meV (Table S3, Supporting Information). Due to its strong excitonic character, the LP only showed a small angle-dependence for all investigated cavities (Figure 4b). Increasing the photonic character of the LP also led to a larger energy shift (0° to 40°) from a minimum of only 11 to 34 meV (Table S3, Supporting Information), which approached the energy shift for purely photonic resonance in a reference cavity without emitter (62 meV). The highest ultrastrong coupling potential $V_A = 386$ meV, which is 30% of exciton energy, was achieved in a c-LEFET with $E_{LP} - E_X = -105$ meV.

In order to gain further insight into the relaxation dynamics of electrically pumped polaritons, the external quantum efficiency (EQE) of the electroluminescence was measured for all c-LEFETs and for a reference LEFET without cavity (Figure S6a, Supporting Information). The samples displayed no or only slight efficiency roll-off, even at ambipolar current densities as high as 4000 A cm^{-2}. Importantly, the ultrastrong coupling regime was maintained for these high current densities. However, despite the fast relaxation of polaritons to the LP branch, the EQE of the c-LEFETs was below the reference LEFET without a bottom mirror, with the most efficient c-LEFET reaching only 30–40% of the reference EQE. Extra optical losses cannot explain this difference because the metal bottom mirror is more

Table 1. Energy E_0, energy shift ΔE_0 and FWHM of lower polariton EL emission (Lorentz fit) at different angles (averaged over ± 1.5°) compared to uncoupled EL and to the lower polariton PL emission (PL LP) at 0° emission angle.

	Uncoupled	PL LP	Electroluminescence lower polariton				
	EL	0°	0°	10°	20°	30°	40°
E_0 [eV]	1.2000	1.2020	1.2034	1.2043	1.2067	1.2105	1.2134
ΔE_0 [meV]	–	–	0	0.9	3.3	7.1	10
FWHM [meV]	360	49	54.7	56.2	54.9	65.7	78.5

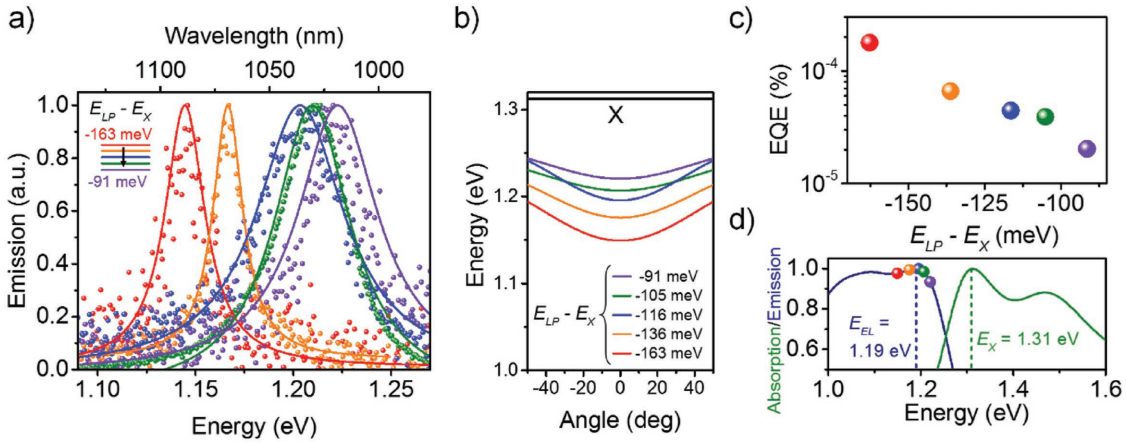

Figure 4. a) Polariton EL emission spectra (with Lorentz fits) in forward direction (at 0°) for different c-LEFETs with varying $E_{LP} - E_X$. b) Lower polariton branches of these c-LEFETs as fitted with the coupled oscillator model. The uncoupled exciton is marked with X. c) EQE of these c-LEFETs at a current density of 750 A cm^{-2} depending on the lower polariton emission energy ($E_{LP} - E_X$). d) Position of the lower polaritons in forward direction for differently detuned c-LEFETs versus the uncoupled excitonic absorption (E_X) and EL emission (E_{EL}).

than 100 nm away from the emission layer and waveguiding can be assumed to be similar in the reference sample, which includes the same AlO_x spacer layer. The reduction of the EQE in cavity OLEDs was previously explained with inefficient population of the LP minimum, either directly from the exciton reservoir or by relaxation along the LP branch.[21,24] As the relaxation, either along the LP branch or directly, showed no bottleneck here and led to a thermalized occupancy, we exclude inefficient population as a loss mechanism. Probably the EQE in c-LEFETs is lower due to incomplete initial scattering from the exciton reservoir into the relaxation paths of the LP. This assumption resembles the concept of active and inactive excitons in the reservoir.[37] Furthermore, bimolecular quenching of exciton-polaritons may contribute to the reduced EQE.[38]

To compare the emission efficiency for different detunings, the EQE at a constant current density (750 A cm^{-2}) is plotted versus $E_{LP} - E_X$ in Figure 4c. The EQE increases with increasing detuning from the exciton transition energy. From the factors comprising the EQE (see Figure S6, Supporting Information), we can derive the scattering (or conversion) efficiency from the exciton reservoir to the LP branch, which follows the same trend as the EQE in Figure 4c. This indicates that the increasing EQE is not solely caused by a rise of the photonic component of the LP with decreasing $E_{LP} - E_X$, but is most likely related to an increased number of excitons that scatter toward the LP branch minimum. Two mechanisms for exciton relaxation have been described: radiative pumping, i.e., radiative recombination of the exciton and reabsorption in the LP, or nonradiative pumping, i.e., scattering of the exciton directly into the LP state, for example, by emission of an excited-state phonon (optical phonon-assisted scattering)[38] or by scattering on a free charge carrier for electrical pumping.[26] The increasing EQE and relaxation efficiency for a red-shift of the LP away from the exciton energy may point to a radiative pumping mechanism.

Figure 4d shows that for the most efficiently emitting cavity the LP is positioned closest to the vibronic shoulder of the emission spectrum at 1.08 eV. Hence more ground state vibrational levels, which assist the radiative pumping, are available. The same trend of increasing quantum efficiency with increasing detuning has been observed for a molecular dye in a polymer matrix, and successfully fitted with a radiative pumping model.[39] Additional phonon-assisted nonradiative relaxation of excitons from the reservoir into the lower exciton-polariton state could possibly play a role for the negatively detuned c-LEFET ($\Delta = -7$ meV), as the energy for relaxation into the LP $E_{LP} - E_X = -163$ meV exactly overlaps with a Raman mode of the BT moiety in the DPPT-BT.[40] Such phonon-assisted scattering was previously observed and modeled for a J-aggregate dye molecule in a polymer matrix.[41] The nonradiative decay mechanism in DPPT-BT might be enhanced by further negative detuning, as more vibrational modes of the thiophene, DPP, and BT units are located at just slightly higher energies of 169–187 meV (1366–1510 cm^{-1}).[40,42] So far there are only a handful examples of polymers showing strong coupling,[7,16,43–45] and further investigation into the particular LP population mechanisms of these materials is highly desirable.

The c-LEFET geometry also enables the investigation of possible effects of (ultra)strong coupling on charge transport in organic semiconductors as proposed by Orgiu et al.[10] Here, we compare the c-LEFET with $E_{LP} - E_X = -163$ meV (i.e., detuning $\Delta = -7$ meV) to an identical reference sample with the same spacer layer but no bottom mirror. The transfer curve for the transistors with a cavity (Figure 1c) shows balanced ambipolar behavior with low hysteresis, this also applies to the reference sample with almost identical transfer characteristics. The corresponding output characteristics (Figure S7, Supporting Information) show almost equal currents for LEFETs with and without cavity. Saturation mobilities and threshold voltages for hole and electron transport were extracted from the transfer characteristics (Figure S8, Supporting Information) for all c-LEFET and reference samples, taking into account the gate voltage dependence of the mobility. The various c-LEFETs with different cavity detuning values did not show significantly different mobilities or threshold voltages than the reference LEFETs (Figure S9, Supporting Information). To further test this result, we investigated the temperature dependence of the field-effect mobility from 170 to 300 K for both transistor samples. The extracted activation energies for

hopping transport were around 46 and 38 meV for holes and electrons, respectively, independent of the presence of a cavity (Figure S10, Supporting Information). We thus conclude that at least for the here investigated range of cavities the ultrastrong coupling regime does not significantly affect charge injection or transport in the high-mobility polymer DPPT-BT.

3. Conclusion

In summary, we presented the integration of an LEFET in a microcavity as a platform for the generation of electrically pumped exciton-polaritons in donor–acceptor polymers. Using DPPT-BT as a semiconducting polymer that combines high ambipolar charge carrier mobilities with high oscillator strength and near-infrared light emission enabled ultrastrong coupling and electrical pumping of polaritons at high current densities. Emission from the ultrastrongly coupled lower polariton was 6.5 times narrower than the uncoupled emission and showed minimal dispersion. Charge transport within the semiconducting polymer and overall electrical device characteristics were unaffected by the presence of the cavity. The robust device characteristics at high electrical pumping rates combined with almost angle-independent polariton electroluminescence without a relaxation bottleneck make cavity-integrated LEFETs a promising platform for future polaritonic devices.

Experimental Section

Cavity-LEFET Fabrication: A top-gate/bottom-contact transistor structure was integrated into a metal-clad microcavity. The bottom cavity mirror consisted of 2 nm Cr and 30 nm Au, evaporated through a shadow mask onto a low sodium glass substrate (Schott AF32 Eco). Subsequently, an aluminum oxide spacer layer was deposited by atomic layer deposition (Ultratech Savannah S100) at 200 °C using trimethylaluminium as precursor and water as the oxygen source. The thickness of this spacer layer, which defined the cavity detuning, was varied between 98 and 390 nm (Table S2, Supporting Information). Two-layer photolithography, electron-beam evaporation of 2 nm Cr/30 nm Au, and lift-off were employed to pattern the source–drain electrodes with channel lengths of L = 5, 10, 20, and 40 µm and channel widths of W = 10 and 5 mm, respectively.

The semiconducting polymer DPPT-BT (poly(2,5-*bis*(2-octyldodecyl)-3,6-*di*(thiophen-2-yl)diketopyrrolo[3,4-*c*]pyrrole-1,4-dione-*alt*-benzo[*c*][1,2,5]thiadiazole)) was purchased from Flexink Ltd (M_n = 33 kg mol^{-1}, M_w = 87 kg mol^{-1}). In order to achieve a film thickness of 60 nm (sample with $E_{LP} - E_X = -105$ meV) or 39 nm (all other samples) solutions of 10 or 8.5 mg mL^{-1} DPPT-BT in chlorobenzene were spin-coated for 60 s at 3000 or 5000 rpm, respectively. Before applying the hybrid gate dielectric, the DPPT-BT films were annealed at 200 °C in a dry nitrogen atmosphere for 30 min to remove water and residual solvent. The hybrid dielectric consisted of PMMA and HfO_x. First, 6 mg mL^{-1} of PMMA (Polymer Source, syndiotactic, M_w = 300 kg mol^{-1}) in anhydrous *n*-butylacetate were spin-coated at 6000 rpm to yield an 11 nm thick film. After annealing at 80 °C, a HfO_x layer was added by atomic layer deposition (Ultratech Savannah S100) at 100 °C using tetrakis(dimethylamino)hafnium as a precursor and water as the oxygen source. The c-LEFET with $E_{LP} - E_X = -105$ meV (98 nm AlO_x, 60 nm DPPT-BT) had a 39 nm layer of HfO_x, while a 51 nm HfO_x layer was deposited on all other samples (39 nm DPPT-BT). Thermally evaporated silver (60 nm) formed the top gate electrode of all transistors and the top mirror of the cavity. The reference samples were fabricated identically to the $E_{LP} - E_X = -163$ meV c-LEFET (140 nm AlO_x, 39 nm DPPT-BT, 11 nm PMMA, 51 nm HfO_x) but either without the bottom mirror (no cavity) or with a 51 nm PMMA layer instead of the DPPT-BT.

Optoelectronic Characterization: Current–voltage characteristics were recorded with an Agilent 4156C Semiconductor Parameter Analyzer or a Keithley 2612A source meter. The maximum ambipolar current density J_d was calculated according to $J_d = \frac{I_d}{W \cdot h}$ from the transistor channel width W = 10 mm, drain current I_d, and assuming a h = 2 nm thick charge accumulation layer. The average saturation mobility was extracted from 12 transistors for each detuning value. Low temperature charge transport measurements were performed in a closed-cycle He-cryostat (Lakeshore CRX-6.5K) from 170 to 300 K in steps of 10 K.

A Fourier imaging setup was employed for angle-resolved measurements as described previously.[4,26] For reflectivity measurements, the light of a calibrated tungsten lamp was focused (spot diameter, ≈3 µm) onto the transistor channel through a near-infrared corrected ×100 objective with 0.8 NA (Olympus LMPL100xIR) and a 50/50 beam splitter. The reflectivity of the cavity was then calculated with respect to a spot next to the cavity where only the top mirror was present. For PL measurements, DPPT-BT was excited by a laser diode (OBIS, Coherent Inc., 640 nm, continuous wave, ≈10 mW) while for EL measurements gate and drain bias were applied. Using the Fourier imaging system, the light reflected/emitted by the LEFET was imaged through a dichroic mirror onto the entrance slit of a spectrometer (Princeton Instruments IsoPlane 320) and detected by a thermoelectrically cooled 640 × 512 InGaAs array camera for the near-infrared regime (Princeton Instruments, NIRvana:640ST) and by a back-illuminated CCD camera for the visible range (Princeton Instruments, PIXIS:400). A long-pass filter (cut-off wavelength, 850 nm) and a linear polarizer were placed in front of the spectrometer. For real space imaging, the same setup was used without the Fourier lens. From the image of the emission zone and the optical resolution limit, the width of the emission zone was estimated to be W_{emz} < 1.1 µm. Using $P = \frac{J_d}{e \cdot W_{emz}}$ the pump rate P was determined from the current density J_d, the elementary charge e, and W_{emz}. Uncoupled EL and PL spectra of the reference LEFET were recorded with an Acton SpectraPro SP2358 spectrometer (grating 150 lines per mm) and a liquid nitrogen-cooled InGaAs line camera (PI Acton OMA V:1024 1.7). The emission was collected through a near-infrared ×50 objective with 0.65 NA (Olympus LCPLN50XIR). The EQE of all LEFETs was measured using a calibrated InGaAs photodiode (Thorlabs FGA21-CAL, active area 3.1 mm^2) as described in detail elsewhere.[18]

Coupled Oscillator Model: The experimentally measured polariton branches were fitted with the coupled oscillator model. By introducing a coupling potential V_A the new eigenstates of the exciton–photon system are given by

$$E_{UP/LP} = 1/2 \cdot \left(E_X - i\hbar\Gamma_X + E_C - i\hbar\Gamma_C\right) \pm \sqrt{V_A^2 + 1/4 \cdot \left(E_X - i\hbar\Gamma_X - \left(E_C - i\hbar\Gamma_C\right)\right)^2}, \quad (1)$$

where E_X is the energy of the excitonic transition having a homogenously broadened half width at half maximum (HWHM) $\hbar\Gamma_X$ and E_C the cavity mode with an HWHM $\hbar\Gamma_C$. The energy dispersion of the cavity is described by

$$E_C(\theta) = E_0\left(1 - \left(\sin(\theta)/n_{eff}\right)^2\right)^{-1/2} \quad (2)$$

for a cavity tuned to $E_0 = E_X + \Delta$ with Δ being the cavity detuning. The effective refractive index n_{eff} was used as a fitting parameter. Because the corresponding cavity mode does not intersect with the exciton, a Rabi splitting cannot be defined here. The photonic (excitonic) fractions of the polariton states were calculated via their projection onto the bare exciton and cavity modes.

Supporting Information

Supporting Information is available from the Wiley Online Library or from the author.

Acknowledgements

M.H. and A.G. contributed equally to this work. The authors thank Dr. Norbert Gulde and Roper Scientific GmbH for the temporary loan of a second IsoPlane 320 spectrograph and a PIXIS camera. This research was financially supported by the European Research Council under the European Union's Seventh Framework Programme (FP/2007-2013)/ERC Grant Agreement No. 306298 (EN-LUMINATE) and under the European Union's Horizon 2020 Framework Programme (FP/2014-2020)/ERC Grant Agreement No. 640012 (ABLASE) and by the EPSRC Programme Grant EP/P030017/1. L.T. thanks EPSRC for support through the CM-DTC (EP/L015110/1). P.C. thanks the DAAD-RISE programme for support. J.Z. thanks the Alfried Krupp von Bohlen und Halbach-Stiftung via the "Alfried Krupp Förderpreis für junge Hochschullehrer" for general support.

Conflict of Interest

The authors declare no conflict of interest.

Keywords

donor–acceptor copolymers, electroluminescence, exciton-polaritons, light-emitting transistors, ultrastrong coupling

Received: September 8, 2017
Revised: November 12, 2017
Published online:

[1] D. G. Lidzey, D. D. C. Bradley, M. S. Skolnick, T. Virgili, S. Walker, D. M. Whittaker, *Nature* **1998**, *395*, 53.
[2] D. G. Lidzey, D. D. C. Bradley, T. Virgili, A. Armitage, M. S. Skolnick, S. Walker, *Phys. Rev. Lett.* **1999**, *82*, 3316.
[3] R. Chikkaraddy, B. de Nijs, F. Benz, S. J. Barrow, O. A. Scherman, E. Rosta, A. Demetriadou, P. Fox, O. Hess, J. J. Baumberg, *Nature* **2016**, *535*, 127.
[4] A. Graf, L. Tropf, Y. Zakharko, J. Zaumseil, M. C. Gather, *Nat. Commun.* **2016**, *7*, 13078.
[5] S. Kéna-Cohen, S. R. Forrest, *Nat. Photonics* **2010**, *4*, 371.
[6] K. S. Daskalakis, S. A. Maier, R. Murray, S. Kena-Cohen, *Nat. Mater.* **2014**, *13*, 271.
[7] J. D. Plumhof, T. Stoferle, L. Mai, U. Scherf, R. F. Mahrt, *Nat. Mater.* **2014**, *13*, 247.
[8] D. Sanvitto, S. Kéna-Cohen, *Nat. Mater.* **2016**, *15*, 1061.
[9] C. P. Dietrich, A. Steude, L. Tropf, M. Schubert, N. M. Kronenberg, K. Ostermann, S. Höfling, M. C. Gather, *Sci. Adv.* **2016**, *2*, e1600666.
[10] E. Orgiu, J. George, J. A. Hutchison, E. Devaux, J. F. Dayen, B. Doudin, F. Stellacci, C. Genet, J. Schachenmayer, C. Genes, G. Pupillo, P. Samorì, T. W. Ebbesen, *Nat. Mater.* **2015**, *14*, 1123.
[11] T. W. Ebbesen, *Acc. Chem. Res.* **2016**, *49*, 2403.
[12] I. Carusotto, C. Ciuti, *Rev. Mod. Phys.* **2013**, *85*, 299.
[13] S. Kéna-Cohen, S. A. Maier, D. D. C. Bradley, *Adv. Opt. Mater.* **2013**, *1*, 827.
[14] T. Schwartz, J. A. Hutchison, C. Genet, T. W. Ebbesen, *Phys. Rev. Lett.* **2011**, *106*, 196405.
[15] S. Gambino, M. Mazzeo, A. Genco, O. Di Stefano, S. Savasta, S. Patanè, D. Ballarini, F. Mangione, G. Lerario, D. Sanvitto, G. Gigli, *ACS Photonics* **2014**, *1*, 1042.
[16] N. Takada, T. Kamata, D. D. C. Bradley, *Appl. Phys. Lett.* **2003**, *82*, 1812.
[17] M. S. Vezie, S. Few, I. Meager, G. Pieridou, B. Dorling, R. S. Ashraf, A. R. Goni, H. Bronstein, I. McCulloch, S. C. Hayes, M. Campoy-Quiles, J. Nelson, *Nat. Mater.* **2016**, *15*, 746.
[18] M. Held, Y. Zakharko, M. Wang, F. Jakubka, F. Gannott, J. W. Rumer, R. S. Ashraf, I. McCulloch, J. Zaumseil, *Org. Electron.* **2016**, *32*, 220.
[19] A. J. Kronemeijer, E. Gili, M. Shahid, J. Rivnay, A. Salleo, M. Heeney, H. Sirringhaus, *Adv. Mater.* **2012**, *24*, 1558.
[20] Tischler Jr., M. S. Bradley, V. Bulovic, J. H. Song, A. Nurmikko, *Phys. Rev. Lett.* **2005**, *95*, 36401.
[21] N. Christogiannis, N. Somaschi, P. Michetti, D. M. Coles, P. G. Savvidis, P. G. Lagoudakis, D. G. Lidzey, *Adv. Opt. Mater.* **2013**, *1*, 503.
[22] M. Mazzeo, A. Genco, S. Gambino, D. Ballarini, F. Mangione, O. Di Stefano, S. Patanè, S. Savasta, D. Sanvitto, G. Gigli, *Appl. Phys. Lett.* **2014**, *104*, 233303.
[23] C. R. Gubbin, S. A. Maier, S. Kéna-Cohen, *Appl. Phys. Lett.* **2014**, *104*, 233302.
[24] S. Gambino, A. Genco, G. Accorsi, O. Di Stefano, S. Savasta, S. Patanè, G. Gigli, M. Mazzeo, *Appl. Mater. Today* **2015**, *1*, 33.
[25] G. H. Lodden, R. J. Holmes, *Appl. Phys. Lett.* **2011**, *98*, 233301.
[26] A. Graf, M. Held, Y. Zakharko, L. Tropf, M. C. Gather, J. Zaumseil, *Nat. Mater.* **2017**, *16*, 911.
[27] P. Sonar, S. P. Singh, Y. Li, M. S. Soh, A. Dodabalapur, *Adv. Mater.* **2010**, *22*, 5409.
[28] T.-J. Ha, P. Sonar, B. Cobb, A. Dodabalapur, *Org. Electron.* **2012**, *13*, 136.
[29] D. Venkateshvaran, M. Nikolka, A. Sadhanala, V. Lemaur, M. Zelazny, M. Kepa, M. Hurhangee, A. J. Kronemeijer, V. Pecunia, I. Nasrallah, I. Romanov, K. Broch, I. McCulloch, D. Emin, Y. Olivier, J. Cornil, D. Beljonne, H. Sirringhaus, *Nature* **2014**, *515*, 384.
[30] Y. Zakharko, M. Held, A. Graf, T. Rodlmeier, R. Eckstein, G. Hernandez-Sosa, B. Hahnlein, J. Pezoldt, J. Zaumseil, *ACS Photonics* **2016**, *3*, 2225.
[31] Y. Zakharko, M. Held, F.-Z. Sadafi, F. Gannott, A. Mahdavi, U. Peschel, R. N. K. Taylor, J. Zaumseil, *ACS Photonics* **2016**, *3*, 1.
[32] M. Held, S. P. Schießl, D. Miehler, F. Gannott, J. Zaumseil, *Appl. Phys. Lett.* **2015**, *107*, 83301.
[33] J. Zaumseil, H. Sirringhaus, *Chem. Rev.* **2007**, *107*, 1296.
[34] M. S. Kang, C. D. Frisbie, *ChemPhysChem* **2013**, *14*, 1547.
[35] D. M. Coles, N. Somaschi, P. Michetti, C. Clark, P. G. Lagoudakis, P. G. Savvidis, D. G. Lidzey, *Nat. Mater.* **2014**, *13*, 712.
[36] M. Furno, R. Meerheim, S. Hofmann, B. Lüssem, K. Leo, *Phys. Rev. B* **2012**, *85*, 115205.
[37] K. G. Lagoudakis, F. Manni, B. Pietka, M. Wouters, T. C. H. Liew, V. Savona, A. V. Kavokin, R. André, B. Deveaud-Plédran, *Phys. Rev. Lett.* **2011**, *106*, 115301.
[38] L. Mazza, S. Kéna-Cohen, P. Michetti, G. C. La Rocca, *Phys. Rev. B* **2013**, *88*, 75321.
[39] R. T. Grant, P. Michetti, A. J. Musser, P. Gregoire, T. Virgili, E. Vella, M. Cavazzini, K. Georgiou, F. Galeotti, C. Clark, J. Clark, C. Silva, D. G. Lidzey, *Adv. Opt. Mater.* **2016**, *4*, 1615.
[40] S. Wood, J.-H. Kim, J. Wade, J. B. Park, D.-H. Hwang, J.-S. Kim, *J. Mater. Chem. C* **2016**, *4*, 7966.
[41] D. M. Coles, P. Michetti, C. Clark, W. C. Tsoi, A. M. Adawi, J.-S. Kim, D. G. Lidzey, *Adv. Funct. Mater.* **2011**, *21*, 3691.
[42] S. Wood, J. Wade, M. Shahid, E. Collado-Fregoso, D. D. C. Bradley, J. R. Durrant, M. Heeney, J.-S. Kim, *Energy Environ. Sci.* **2015**, *8*, 3222.
[43] D. Urbonas, T. Stöferle, F. Scafirimuto, U. Scherf, R. F. Mahrt, *ACS Photonics* **2016**, *3*, 1542.
[44] R. F. Oulton, N. Takada, J. Koe, P. N. Stavrinou, D. D. C. Bradley, *Semicond. Sci. Technol.* **2003**, *18*, 419.
[45] L. Tropf, C. P. Dietrich, S. Herbst, A. L. Kanibolotsky, P. J. Skabara, F. Würthner, I. D. W. Samuel, M. C. Gather, S. Höfling, *Appl. Phys. Lett.* **2017**, *110*, 153302.